Available online at www.sciencedirect.com
ScienceDirect
Advances in Water Resources 30 (2007) 1408–1420
Advances in Water Resources
www.elsevier.com/locate/advwatres

Magnetic resonance microscopy of biofouling induced scale dependent transport in porous media

Joseph D. Seymour [a,c,*], Justin P. Gage [a,c], Sarah L. Codd [b,c], Robin Gerlach [c]

[a] Department of Chemical and Biological Engineering, Montana State University, 306 Cobleigh Hall, P.O. Box 59717, Bozeman, MT 59717-3920, USA
[b] Department of Mechanical and Industrial Engineering, Montana State University, Bozeman, MT 59717-3920, USA
[c] Center for Biofilm Engineering, Montana State University, Bozeman, MT 59717-3920, USA

Received 7 July 2005; received in revised form 24 October 2005; accepted 5 May 2006
Available online 22 September 2006

Abstract

Non-invasive magnetic resonance microscopy (MRM) methods are applied to study biofouling of a homogeneous model porous media. MRM of the biofilm biomass using magnetic relaxation weighting shows the heterogeneous nature of the spatial distribution of the biomass as a function of growth. Spatially resolved MRM velocity maps indicate a strong variation in the pore scale velocity as a function of biofilm growth. The hydrodynamic dispersion dynamics for flow through the porous media is quantitatively characterized using a pulsed gradient spin echo technique to measure the propagator of the motion. The propagator indicates a transition in transport dynamics from a Gaussian normal diffusion process following a normal advection diffusion equation to anomalous transport as a function of biofilm growth. Continuous time random walk models resulting in a time fractional advection diffusion equation are shown to model the transition from normal to anomalous transport in the context of a conceptual model for the biofouling. The initially homogeneous porous media is transformed into a more complex heterogeneous porous media by the biofilm growth.

Keywords: NMR; MRI; Biofouling; Biofilms; Porous media; Anomalous transport

1. Introduction

Experimental data on the impact of biological activity on transport in porous media in three dimensions has been limited to bulk measurements of pressure drop and tracer breakthrough curves [1,2]. Magnetic resonance (MR) methods provide the ability to non-invasively monitor transport processes and biomass accumulation and distribution [3–6]. The application of MR methods to study environmental science (special issue J Env Qual 2002;31(2)) and biological activity in porous systems [3] has been reviewed. MR studies of transport reported in the hydrology literature have tended to focus on application of spatially resolved velocity imaging [7–9] from which the permeability can be rigorously determined [10]. In this paper, a short overview of the measurement of scale dependent dispersion dynamics by pulsed gradient spin echo (PGSE) MR is given, as much of the research in this area has been reported in the physics, engineering and MR literature [11–18].

The analysis of bioactivity applying these scale dependent techniques, provides quantitative measurement of the change in hydrodynamic dispersion dynamics due to biofouling [6]. The MR data indicate a transition caused by biofilm growth, from normal Gaussian dynamics due to a Fickian dispersion process for flow through the homogenous model media, to anomalous non-Gaussian dynamics [19–21] due to non-Fickian dispersion [6]. The data is discussed in the context of fractional advection dispersion equations and indicate the applicability of continuous time random walk (CTRW) theory to model the transition [22–25]. The biofilm growth alters the homogeneous porous media system structure, increasing the system complexity

* Corresponding author. Tel.: +1 406 9946853; fax: +1 406 9945308.
E-mail address: jseymour@coe.montana.edu (J.D. Seymour).

0309-1708/$ - see front matter © 2006 Elsevier Ltd. All rights reserved.
doi:10.1016/j.advwatres.2006.05.029

[26] and transforming the porous media into a heterogeneous system. The dispersion data presented, clearly indicate the ability of displacement scale dependent PGSE MR methods to characterize anomalous transport [27].

2. Hydrodynamic dispersion

The classic theory of hydrodynamic dispersion in porous media is based in large part on the work of G.I. Taylor who first derived the celebrated Ornstein–Uhlenbeck process of stochastic dynamics [28,29]. Taylor later demonstrated that coarse graining [30] through averaging of continuum models results in effective Brownian motion processes [31,32]. The fundamental aspect of models of dispersion in porous media is the resultant advection diffusion equation (ADE) governing mass, or probability, conservation in the system. An effective diffusion coefficient, *i.e.* dispersion coefficient, dependent upon the fluctuations about the mean velocity, quantifies transport in the system. Many theoretical approaches to derive the conservation equation and the corresponding transport coefficients have been applied and result in consistent governing equations [33].

Averaging of the continuum mass conservation equations using generalized macrotransport theory based on the method of moments [34] and stochastic process methods based on the central limit theorem [35], return the classical ADE. The ADE is applicable to homogeneous porous media systems in which the dynamics are Gaussian in the asymptotic time limit. In this case the dispersion coefficient is a constant and the mean squared displacement, or positional variance, scales linearly in time. In systems in which long range correlations in the transport dynamics occur due to the heterogeneous nature of the porous media system, non-local transport theories based on ensemble averaging of the continuum momentum and mass conservation equations [36] and nonequilibrium statistical mechanics [37], among other methods, have been applied. Dispersion coefficients in the non-local formulation are dependent on the displacement length and time scale and result in a mean squared displacement which scales non-linearly in time, the definition of anomalous diffusion [38]. More recently transport in heterogeneous porous media has been modeled using the theory of CTRWs which lead to fractional advection diffusion equation (FADE) mass conservation models [19,20,25].

2.1. Normal diffusion: ADE

The theory of Brownian motion involves the averaging or coarse graining of fast variables in a system, a separation of scales [30]. In the case of a colloidal particle suspended in a liquid, the velocity fluctuations of the particle occur rapidly relative to the position variation and the treatment results in a Fokker–Planck, or Smoluchowski equation, governing the particle concentration or probability [32]. As indicated above, the long time asymptotic behavior of the process is Gaussian with a constant effective diffusion, *i.e.* dispersion, coefficient, and linear scaling of the mean squared displacement in time. In the non-asymptotic short time regime the time dependence of the mean squared displacement is quadratic in time consistent with the ballistic motion of a particle with a constant velocity. The Brownian motion process has been solved for full time dependence and is the Ornstein–Uhlenbeck stochastic process [28–30]. Preasymptotic time dependence of the normal Brownian motion diffusion process, during which the mean squared displacement transitions from the short time quadratic time scaling behavior of the ballistic regime, to the long time linear scaling of the diffusive regime, to the long time linear scaling of the diffusive regime, is in contrast to anomalous diffusion in which non-linear time scaling of the mean squared displacement persists for asymptotic times [21,38].

The mass, or probability, conservation equation for axial z-direction flow in a porous media is given by the ADE

$$\frac{\partial P(Z,t)}{\partial t} = \left[-\langle v_z\rangle \frac{\partial}{\partial Z} + D^* \frac{\partial^2}{\partial Z^2}\right] P(Z,t). \tag{1}$$

The time rate of change of the probability of a tracer, or solute particle (molecule) $P(Z,t)$ having displacement Z in time t is dependent on the advection due to the mean velocity $\langle v_z\rangle$ and the dispersion coefficient D^*. The ADE is Galilei invariant, meaning the distribution is invariantly translated with the average velocity. The effective diffusion, or dispersion, coefficient depends on the velocity fluctuation autocorrelation function $D^*(\Delta) = \int_0^{\Delta}(1-\frac{\tau}{\Delta})\langle[v_z(t+\tau)-\langle v_z\rangle][v_z(t)-\langle v_z\rangle]\rangle\,\mathrm{d}\tau$ and can be written in time dependent fashion where Δ is the observation time scale [30]. The effective diffusion for the time dependent Brownian motion Ornstein–Uhlenbeck process is recovered for an exponential velocity fluctuation autocorrelation. In the asymptotic limit, for times Δ much larger than the correlation time of the process, $D^* = \lim_{\Delta\to\infty} D^*(\Delta) = \int_0^{\infty}\langle[v_z(t+\tau)-\langle v_z\rangle][v_z(t)-\langle v_z\rangle]\rangle\,\mathrm{d}\tau$ and the mean squared displacement of the solute or tracer in the long time limit is $\langle Z(t)^2\rangle - \langle Z(t)\rangle^2 = 2D^*t$. The random fluctuations in velocity about the mean velocity at the pore scale generate an effective Brownian motion diffusion process at the macroscopic scale. In classical continuum modeling of porous media transport it is the averaging of the continuum equations of conservation of mass and momentum which provides the coarse graining that results in the Brownian motion nature of the model.

2.2. Anomalous diffusion: FADE model of biofouling

The separation of scales which occurs in development of the Brownian motion theory is the reason the ADE fails to model macroscopic transport in systems with heterogeneity over many scales. Correlated dynamics are generated by the heterogeneities in structure and corresponding transport properties, *e.g.* permeability, that results in non-local

or memory effects. CTRW theory provides a basis for modeling anomalous transport generated by the correlated dynamics [21,38,39] and is equivalent to a mass, or probability, conservation approach based on generalized master equations [25,40–42] from which fractional ADE's can be derived [23]. The CTRW approach is consistent with non-local continuum mechanics [36] and non-equilibrium statistical mechanics [43] models for transport in heterogeneous porous media.

CTRWs characterize transport in terms of a jump probability distribution $\psi(Z,t)$ for a tracer particle to undergo a jump Z after waiting time t. Transport equations which are fractional in either space or time are derived by assuming independence of the jump length $\lambda(Z)$ and waiting time $w(t)$ distributions so that $\psi(Z,t)=\lambda(Z)w(t)$. Normal diffusion, or Brownian motion, is recovered for finite mean waiting times and jump length variances. Anomalous diffusion is obtained in the form of a time FADE for divergent mean waiting time and a space FADE for divergent jump length variances, corresponding to power law wait time and jump length distributions respectively [21,23]. Discussion of the applicability of the space fractional and time fractional forms of FADEs to modeling transport in heterogeneous subsurface environments has recently been discussed in detail [25].

In the case of constant velocity systems the fractional operator functions only on the diffusive term and the FADEs are Galilei invariant [21,24]. The theory applied to analyze the MR measured transition in the dispersion dynamics due to biofilm growth is a time fractional model. The fluid particles, in our case the water molecules on which the MR active ^{1}H protons reside, have a power law distribution of wait times and molecular jumps independent of the preceding wait time but dependent on the velocity at the starting point and the average time of flight [23,24]. This model accounts for varying spatial distributions of velocity and is Galilei variant [21,23,24]. The conceptual model of the biofilm impacted porous media is that the water molecules have a power law distribution of wait times due to heterogeneous trapping over a hierarchy of scales. At the molecular level of the extracellular polymeric substance (EPS) hydrogel matrix which composes the biofilm, heterogeneity manifests itself in regions of varying polymer density and corresponding water mobility [44,45]. At the pore scale the distribution of biomass from pore to pore is heterogeneous with pores ranging from fully blocked to clean generating a heterogeneous permeability field. Water molecules trapped in the biomass or fluid in blocked and partially blocked pores must diffuse or slowly flow out to join the faster moving fluid and have long wait times, while molecules in minimally blocked or clean pores have shorter or non-existent wait times.

A power law Levy stable wait time distribution, $w(t)\sim t^{-1-\alpha}$, for $0<\alpha<1$ leading to divergent mean wait time and a Gaussian jump length distribution with finite variance and starting velocity dependent shift are applied [21,23,24]. The result is the time FADE,

$$\frac{\partial P(Z^*,t^*)}{\partial t^*}={}_0\mathbf{D}_t^{1-\alpha}\left[-A_\alpha\frac{\partial}{\partial Z^*}v(Z^*)+D_\alpha\frac{\partial^2}{\partial Z^{*2}}\right]P(Z^*,t^*) \tag{2}$$

where A_α is a derivation based advection parameter and D_a is the effective diffusion, or dispersion coefficient [21,23,24]. The superscript star notation is adopted to indicate the dimensionless space–time variables associated with the model space in contrast to real space associated with the MR measurements. The fractional Riemann–Liouville operator is defined as

$${}_0\mathbf{D}_t^{1-\alpha}P(Z^*,t^*)=\frac{1}{\Gamma(\alpha)}\frac{\partial}{\partial t^*}\int_0^{t^*}\frac{P(Z^*,t')}{(t^*-t')^{1-\alpha}}\,\mathrm{d}t'. \tag{3}$$

Note that for $\alpha=1$ the Riemann–Liouville operator is unity, Eq. (2) becomes the normal ADE and Gaussian statistics are obtained. In order to provide graphical representation of the time FADE and make qualitative connection to the MR data the tractable model of a constant velocity $v^*=A_\alpha v$ is applied. The mean squared displacement then takes the form

$$\left\langle Z(t^*)^2\right\rangle-\langle Z(t^*)\rangle^2=\frac{2D_\alpha}{\Gamma(1+\alpha)}t^\alpha+(v^*)^2t^{2\alpha}\times\frac{2\Gamma^2(1+\alpha)-\Gamma(1+2\alpha)}{\Gamma^2(1+\alpha)\Gamma(1+2\alpha)} \tag{4}$$

in which the $t^{2\alpha}$ scaling results from the increased spreading due to the variations in velocity as in Taylor dispersion [23,24,46–48].

3. Magnetic resonance

3.1. MR microscopy of biomass and velocity

The MRM pulse sequence used to obtain biofilm contrast is a magnetic spin–spin relaxation time weighted spin-warp sequence in which the spins in the slice of interest ($z=-s/2$ to $s/2$) are excited at an initial time with a 90° radio frequency (rf) pulse, Fig. 1(a) [49]. Gradients in the x and y direction are stepped such that for each gradient value, spins acquire a magnetization phase shift dependent on their location. The signal is dephased and refocused at effective echo times of $1t_e$, $2t_e$, $3t_e$...$8t_e$ [50]. The MR signal, $S(k_x,k_y,t_e)$ obtained at each echo time is the Fourier inversion of the spin density, $\rho(x,y,z)$ weighted by the average relaxation time parameter $T_2(x,y,z)$ at each image voxel

$$S(k_x,k_y,t_e)=\int_{-s/2}^{s/2}\left[\int_{-\infty}^{\infty}\int_{-\infty}^{\infty}\exp\{-t_e/T_2(x,y,z)\}\rho(x,y,z)\times\exp\{\mathrm{i}2\pi(k_xx+k_yy)\}\,\mathrm{d}x\,\mathrm{d}y\right]\mathrm{d}z \tag{5}$$

Here $k_i=(2\pi)^{-1}\gamma G_i\tau$ is the Fourier reciprocal wavelength to position and τ is the duration of the gradient of amplitude G_i in the i-direction. In the spin warp imaging sequences of Fig. 1(a) and (b) the x gradient is the phase encode gradient in which spatial resolution is obtained by

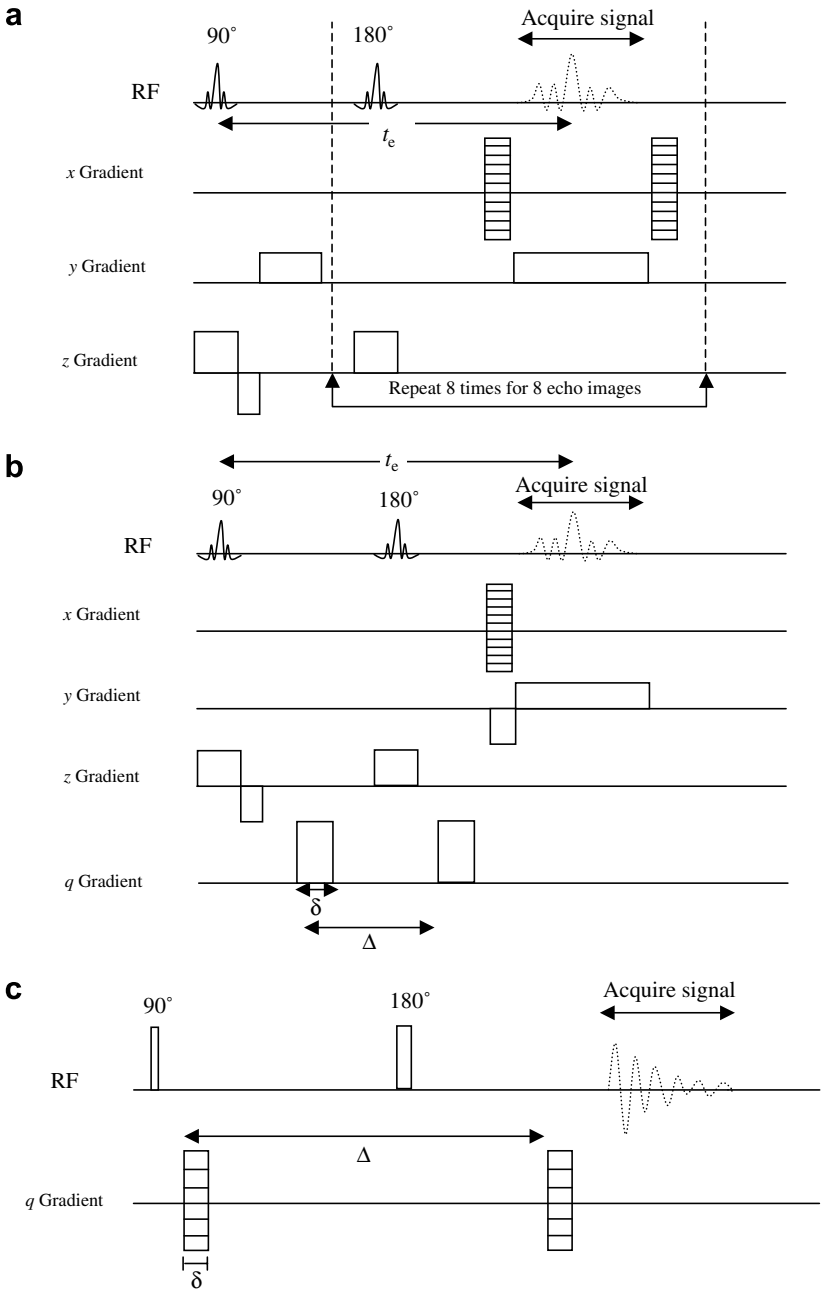

Fig. 1. Pulse sequence or timing diagram indicating the application of radio frequency excitation pulses and magnetic field gradients. (a) To make a T_2 map the echo image is reproduced eight times at different values of t_e. A map representing the decay rate of the signal in each image voxel distinguishes short T_2 spins experiencing restricted motion in the biofilm from long T_2 spins experiencing free diffusion in the bulk fluid. (b) To make a velocity map the echo image is repeated with different values of the q gradient pulse pair which generates a velocity sensitive phase shift in the magnetization at each image voxel. (c) Pulsed gradient spin echo pulse sequence for generation of the propagator, or conditional displacement probability $P_s(Z, \Delta)$. The sequence samples all of the Fourier reciprocal wavelength space to displacement, q space, with positive and negative q values in order to construct artifact free propagators by Fourier transformation. The data obtained is dependent on the displacement wavelength q and sampling time Δ.

incrementing the amplitude G_x, while the y gradient is the frequency encode gradient for which $\tau = N\Delta t$ is incremented during signal acquisition for fixed G_y. Fourier transformation of the MR signal provides the relaxation weighted spin density $\rho(x, y)$ spatially averaged over the slice thickness in z. Each gradient can be applied along any coordinate axis providing an image of differing spatial orientation.

Velocity maps are obtained using the spin-warp slice selection sequence, with a pair of gradient pulses added to encode for molecular motion [49]. The motion encoding gradient pulses are located either side of the refocusing 180° pulse, Fig. 1(b). The first gradient pulse encodes the spins with a phase in magnetization dependent on their location at that point in time, and the second gradient pulse reverses this phase encoding. If a spin moves in the time

period Δ, the spin retains a residual phase shift directly proportional to the displacement that has occurred in the time interval Δ. The MR spin echo signal normalized to eliminate relaxation effects, $E(k_x,k_y,q) = S(k_x,k_y,q)/S(k_x,k_y,q=0)$, is the Fourier inversion of the density of the spins weighted by the coherent motion

$$E(k_x,k_y,q_i) = \int_{-s/2}^{s/2}\left[\int_{-\infty}^{\infty}\int_{-\infty}^{\infty}\exp\{-\mathrm{i}2\pi\Delta q_i v_i(x,y,z)\}\rho(x,y,z) \times \exp\{\mathrm{i}2\pi(k_x x + k_y y)\}\,\mathrm{d}x\,\mathrm{d}y\right]\mathrm{d}z \quad (6)$$

The Fourier reciprocal wavelength to displacement is $q_i = (2\pi)^{-1}\gamma g_i\delta$, and δ is the duration of the velocity encoding gradient of magnitude g_i applied in the i-direction. A map of the residual phase shift at each spatial location provides an image of the average velocity over time Δ in each image pixel. Additional time averaging of the velocity occurs during the order of 10 min to acquire the velocity map, so each pixel provides the stationary velocity at that spatial location [51]. The full propagator, discussed in the next section, can be measured at each point in the image by incrementing the wave vector q [49].

3.2. MR measurement of dispersion

Motion is measured by the pulsed gradient spin echo (PGSE) experiment [49,52] consisting of gradient pulses g of duration δ, on each side of a π rf pulse separated by time Δ, Fig. 1(c). Displacements on the order of magnitude of 10 nm–10 mm on timescales from 100 μs to 1 s can be measured. The first gradient pulse generates a phase of spin magnetization for each group of spins at a given position. Individual spins translate for time Δ and the second gradient pulse unwraps the phase. The residual phase shift due to change in position between the gradients provides displacement over time Δ, measuring velocity of the spins. To the extent the spins experience random motion over time Δ, the NMR signal is attenuated through dephasing caused by unequal unwrapping of the phases. This is the basis for measurement of effective diffusion, or dispersion. The signal detected in a PGSE experiment without spatial resolution for the gradient in the z-direction is

$$E(q,\Delta) = S(q,\Delta)/S(q=0,\Delta) = \int P(Z,\Delta)\exp[\mathrm{i}2\pi qZ]\,\mathrm{d}Z \quad (7)$$

The wave vector $q = (2\pi)^{-1}\gamma g\delta$, is the Fourier reciprocal variable to displacement $Z = z'(\Delta) - z(0)$. Fourier transformation of the echo signal acquired for incremented values of q, obtained by stepping g, is the averaged propagator $P(Z,\Delta) = \int \rho(x,y,z)P_s(z,0|z',\Delta)\,\mathrm{d}x\,\mathrm{d}y\,\mathrm{d}z$. This quantity is the average over the initial spin distribution $\rho(x,y,z)$, of the van Hove self-correlation function [53], or conditional probability $P_s(z,0|z',\Delta)$, that a spin residing at r at time 0 moves to z' at time Δ [49]. A normal diffusion process described by Gaussian statistics with average velocity $\langle v_z\rangle$ and g along the z-direction has an average propagator $P(Z,\Delta) = (4\pi D\Delta)^{-1/2}\exp[-(Z-\langle v_z\rangle\Delta)^2/(4D\Delta)]$ and results in a measured signal of the form $E(q,\Delta) = \exp(\mathrm{i}2\pi q\Delta\langle v_z\rangle)\exp(-4\pi^2q^2D\Delta)$. Here it is clear the signal phase is modulated by the mean velocity and it is attenuated by diffusion. If the propagator is non Gaussian due to anomalous or preasymptotic effects, PGSE NMR measures spin displacement wavelength q and time Δ dependence.

The wavelength and time dependence of dispersion are characterized by the PGSE data in calculation of the full propagator. This is done by sampling the entire q-space at varying displacement times Δ to obtain the propagator for each time [12,14,15,47]. In the asymptotic time limit Gaussian propagators are recovered for dispersion in homogeneous porous media, demonstrating the applicability of the Brownian motion models and the normal ADE. Analysis of the PGSE data in the q-space as a function of displacement times allows for analogies to neutron scattering and diffraction like effects, due to restricted diffusive motion in uniform pore spaces and provides structural detail on the system [48,49,54]. Flow in porous media with uniform pore spaces generate q-space plots that exhibit diffraction like effects due to the magnetization coherence generated by the ensemble of spins as they translate the uniform pore space and are indicators of structural regularity [11,17,48]. Applying the method of Stejskal and Tanner [52] and fitting the low q regime of the data as a function of observation time Δ provides $D^*(\Delta)$ [11,15]. The approach to the asymptotic regime in model porous media flow show agreement with the Ornstein–Uhlenbeck process and have been compared to Lattice–Boltzmann simulations [15,16,55,56].

3.3. Advanced techniques

The PGSE method is the simplest manifestation of the pulsed gradient techniques to measure scale dependent deterministic and random motion. Multiple gradient methods provide the ability to determine multiple displacement directional correlations [16,57], velocity time and directional correlations [58], frequency dependent dispersion [59] and velocity autocorrelation functions [60,61]. In addition rapid 'single shot' techniques for the measurement of effective diffusion and flow provide the means to acquire complete data in the millisecond time scale to study transient behavior [62,63]. Of particular application to the study of bioactivity in porous media are new techniques for the measurements of 2-D correlations of magnetic relaxation time and effective diffusion [64–66]. These 2D MR parameter correlation methods provide the potential for unique data on the relation between the structure of the biofilm and the transport processes. All of these advanced methods have the potential to provide additional detail on the dynamics of anomalous transport transition induced by biofouling presented here.

4. Experimental details

4.1. Model bead pack and microbiology

A 5 mm i.d. porous media column packed bed reactor was constructed using 241 μm diameter monodisperse polystyrene beads (Duke Scientific 4324A). Experiments utilized a dual syringe pump (Pharmacia P-500) which allows controlled volumetric flow rates. The column, tubing and pump were sterilized by repeated treatments with an ethanol solution (70% wt). For bacterial experiments, the column was then inoculated with a strain of *Pseudomonas aeruginosa* (FRD1 containing the plasmid PAB1) [67]. The system was kept for approximately 10 h under very low flow (10 ml/h) of a 1/10 dilution of tryptic soy broth (TSB) media (Becton Dickinson) to allow initial bacterial attachment to the beads. The column was then aseptically transferred to the MR system. Either de-ionized water for the non-bacterial experiments or 1/10 TSB media under constant stirring to ensure oxygenation was pumped into the column from bottom to top with the effluent collected in a waste carboy. Magnevist® (Berlex Laboratories) was added to the de-ionized water and 1/10 TSB media at 0.05% vol/vol. The addition of Magnevist® causes faster magnetic relaxation resulting in shorter image acquisition times. The temperature of the column was held constant at 20 °C for all data collection. The temperature was increased daily for several hours in the bacterial experiments to 37 °C to encourage biofilm formation and growth.

4.2. MR experiments

The sample was placed through an 8 mm gradient coil in a 250 MHz vertical standard bore superconducting magnet. A Bruker Avance DRX spectrometer was networked to the superconducting magnet. A Bruker Micro5 microimaging probe and gradient amplifiers were used which allowed imaging using gradient coils capable of 2 T/m in all three spatial directions. A series of MR pulse sequences were repeated over a 7–10 day period to monitor the effects of biofilm growth on T_2 spin–spin magnetic relaxation, velocity distributions, and averaged propagators. T_2 maps were generated using the pulse sequence of Fig. 1(a) collecting eight echo images with an echo time TE = 10 ms, 20 ms up to 80 ms and a repetition time TR = 500 ms with a total acquisition time of around 40 min. Velocity maps were acquired with the pulse sequence of Fig. 1(b) using the experimental parameters $\Delta = 6$ ms, $\delta = 1$ ms, TE = 17.9 ms and TR = 2 s with 0 and 0.08 T/m gradient values. The total velocity imaging time was approximately 70 min. The PGSE pulse sequence, Fig. 1(c), was used to measure the echo signal, $E(q,\Delta)$ and to compute the averaged propagators $P(Z,\Delta)$. The experimental parameters used for these experiments were a repetition time TR = 2 s, an echo time TE $\sim \Delta$ and $\delta = 1$ ms. 128 q sampling points were used within the range of gradient values of $-g_{\max}$ to $+g_{\max}$ in order to fully sample the q-space and avoid artifacts due to undersampling of the displacements [48]. The maximum gradient value, $g_{\max}$, was chosen in order to prevent data aliasing and varied depending on the value of Δ ranging from 0.2 T/m for $\Delta = 300$ ms to 0.5 T/m for $\Delta = 20$ ms. The total acquisition time for 128 point sampling was approximately 35 min.

4.3. Generation of FADE

An integral form for the time FADE propagator is described in Metzler and Compte [24] for the normalized case of dimensionless advection $v^* = 1$ and diffusion $D^*_\alpha = 1$, as

$$P_\alpha(Z^*,t^*) = \int_0^\infty A(s,t^*)\frac{1}{\sqrt{4\pi t^*}}\exp\left(-\frac{(s-t^*)^2}{4t^*}\right)\mathrm{d}s \qquad (8)$$

where the kernel $A(s,t^*)$ is given as the inverse Laplace transform

$$A(s,t^*) = \angle^{-1}\left\{u^{\alpha-1}\exp\left(-su^\alpha\right)\right\}. \qquad (9)$$

Our graphical representations of the FADE were generated using a series expansion approximation of the kernel $A(s,t)$ given in Metzler and Klafter [21]

$$A(s,t^*) = \frac{1}{s}\sum_{n=0}^{\infty}\frac{(-1)^n}{\Gamma(1-\alpha-\alpha n)\Gamma(1+n)}\left(\frac{s}{(t^*)^\alpha}\right)^{1+n}. \qquad (10)$$

This series representation was evaluated in Mathematica for α= 1, 2/3, 1/2 and 1/10 giving solutions for $A(s,t^*)$ in terms of gamma and hypergeometric functions. The integral representation of the FADE propagator, Eq. (8), was evaluated for each Z^* value in MATLAB by summing over s values until the sum converged.

5. MR measurements

5.1. Magnetic relaxation and velocity imaging

MRM images of the pore scale spin–spin T_2 magnetic relaxation time and velocity as a function of biofilm growth are shown in Fig. 2. The T_2 relaxation time is dependent on the molecular rotational mobility which controls dipole–dipole interactions among the spins. Highly mobile molecules average out the dipolar interaction resulting in a longer T_2 relaxation time and slow relaxation rate while restricted mobility increases the dipolar interaction and generates a fast relaxation rate and short T_2 [49]. Water molecules within the biofilm EPS hydrogel matrix and cell clusters have restricted mobility and provide an indicator of biomass through a decrease in T_2 [44,45]. The variation in T_2 as a function of biofilm growth from Day 1 to Day 7 is clearly indicated in the images and histograms. Note the increasing heterogeneity in the T_2 image and histogram. The velocity images indicate significant variation in the pore scale velocity due to biofilm growth [6]. The Day 1 image of the clean bead pack shows significant velocity in the 3–4 mm/s range distributed fairly uniformly. The

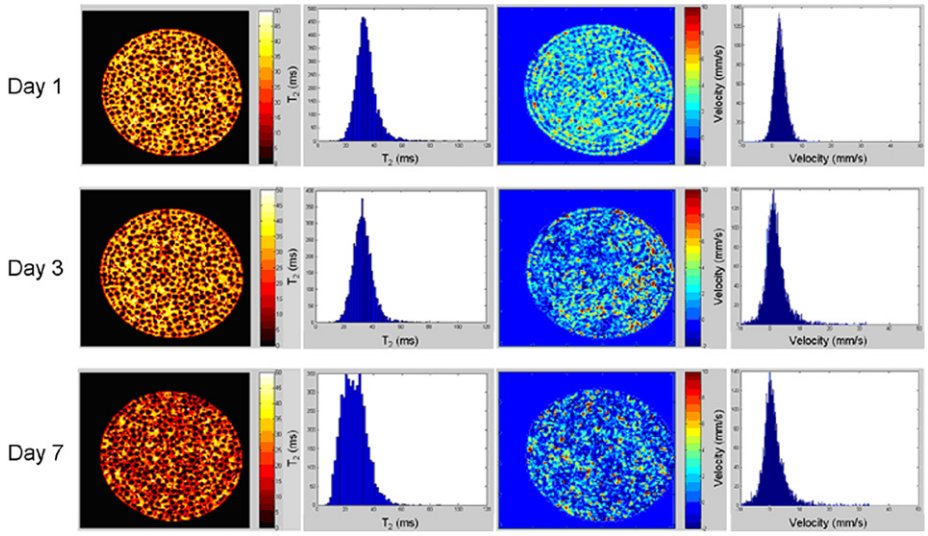

Fig. 2. T_2 (first column) and velocity (third column) maps with histograms as a function of biofilm growth from the clean bead pack on Day 1. The velocity maps are taken under flow conditions with an average tube velocity of 1.42 mm/s while the T_2 maps are obtained without flow. Spatial resolution is 54.7 μm/pixel (128 × 128 pixels) in plane over a 1000 μm slice for velocity and a 200 μm slice for T_2. The T_2 map is proportional to biomass with white-yellow color indicating highly mobile free water, red–orange indicating less mobile water within the biomass and black indicating the polymer beads composing the pack. Note the T_2 histogram vertical axis scale decreases as biofilm growth generates a broader distribution from Day 1 to 7. The velocity color bar ranges from red, 10 mm/s, to blue (background), 0 mm/s, and dark blue, −2 mm/s.

Day 1 histogram is centered about 1.4 mm/s and is narrowly distributed indicating homogeneity. The velocity image for Day 3 indicates a significant alteration of the pore scale velocity with regions of very fast flow and very slow or even slightly negative velocity and a broadening and shift to slower velocity of the histogram. The variation in velocity is more apparent by Day 3 than the T_2 relaxation variation demonstrating the ability of MR motion sensitive measurements to indicate biomass. By Day 7 the velocity image indicates a heterogeneous pore scale distribution of velocity with a corresponding broadening of the histogram and the appearance of more pores with very high velocity and a further shift of the histogram toward 0 mm/s, indicating the increase in biofilm clogged pores.

5.2. Preasymptotic dispersion

In order to characterize the dispersion in the clean bead pack of Day 1 the propagator as a function of the displacement time Δ was measured and is shown in Fig. 3. The

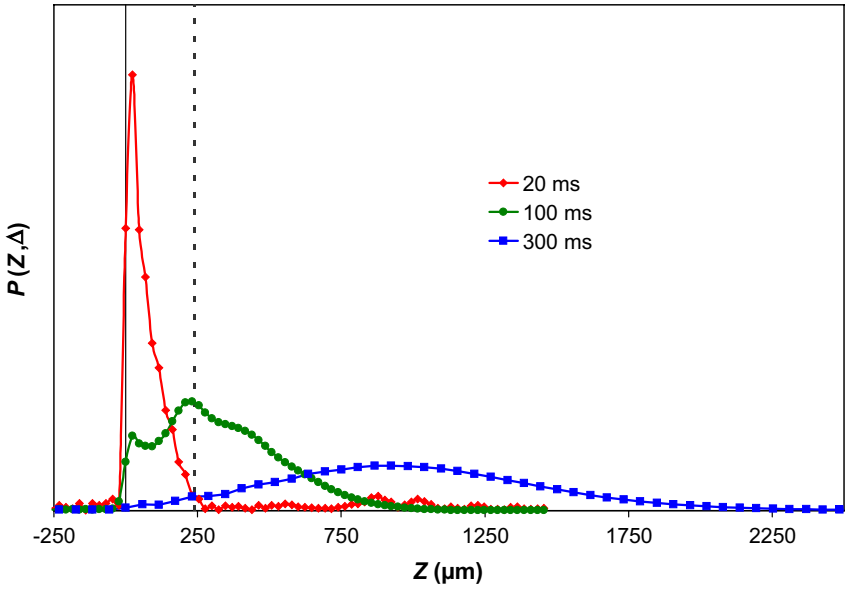

Fig. 3. Propagators of motion for the axial displacement for a clean bead pack as a function of displacement observation time Δ taken under flow conditions with an average tube velocity of 1.42 mm/s. The vertical dashed line indicates the monodisperse particle diameter of 241 μm.

propagator shows the approach to the asymptotic Gaussian behavior corresponding to the normal ADE. The propagator at 20 ms indicates few if any water molecules have left the pore in which they started, displacing less than the pore size which is taken as the monodisperse bead size of 241 μm. By 100 ms some water molecules have displaced further than a single pore and the propagator shows a slight peak around the pore size. After 300 ms all the water molecules have sampled multiple pores undergoing mechanical and Taylor dispersion and the propagator is clearly a Gaussian offset to the mean displacement. The MR propagator data provide direct measurement of the temporal approach to the Gaussian normal diffusion process and clearly indicate the applicability of the Galilei invariant ADE.

5.3. Biofilm growth induced transition to anomalous dispersion

The impact of biofilm growth on macroscale transport dynamics can be quantified by measuring the propagator as a function of biofouling. Fig. 4 shows the propagators for $\Delta = 300$ ms on linear, Fig. 4(a), and log, Fig. 4(b), scales. The propagators clearly show the transition of the dispersion dynamics from Galilei invariant Gaussian behavior, Day 1, to Galilei variant non-Gaussian behavior, Day 3 and 7 [6]. The Day 3 data has a pronounced peak around zero displacement within the pore length due to the trapping of water molecules within the biomass and the increase in clogged pores. In order to conserve mass under the constant volumetric flow rate conditions of the

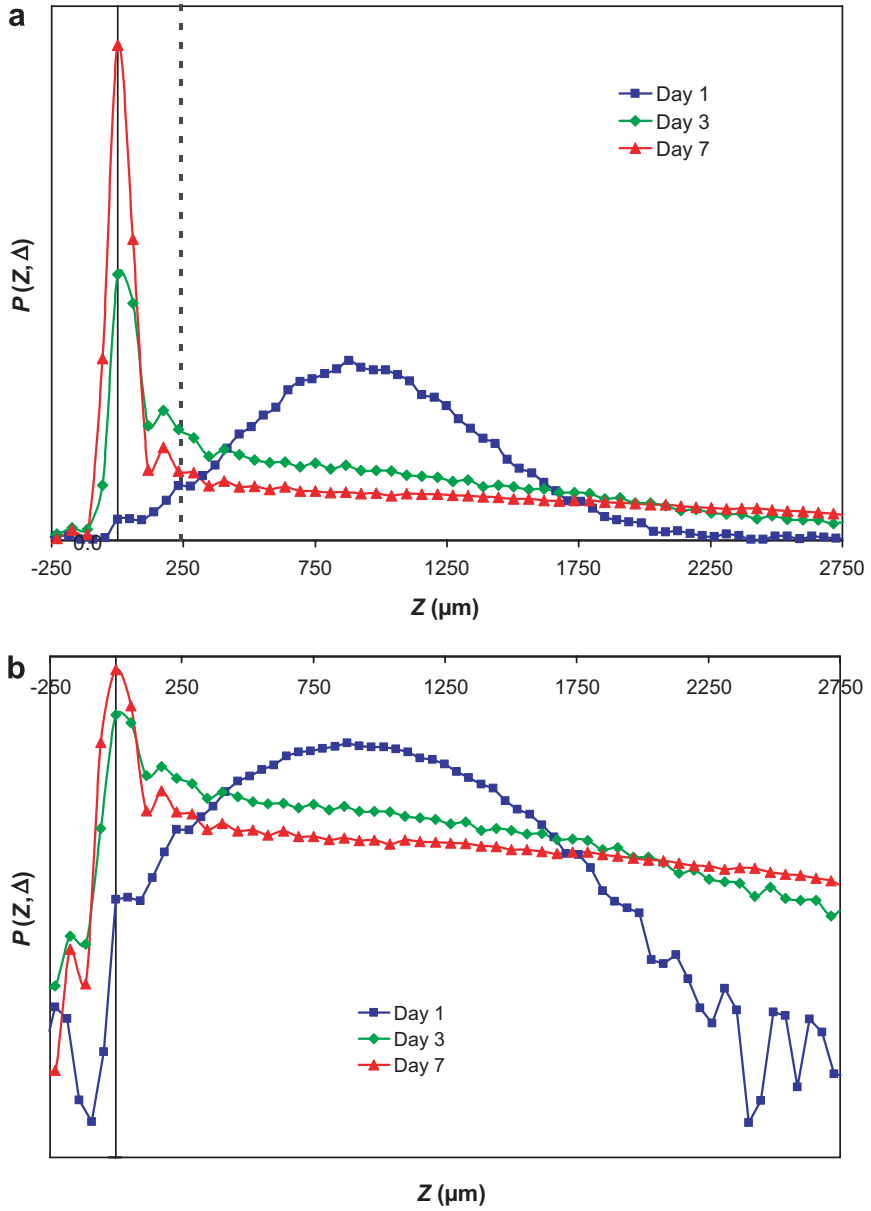

Fig. 4. Propagators of motion for the axial displacement for displacement observation time $\Delta = 300$ ms as a function of biofilm growth in linear (a) and log (b) scale taken under flow conditions with an average tube velocity of 1.42 mm/s.

experiment, more water molecules undergo large displacements as pore clogging occurs, resulting in a large displacement tail in the distribution. The Day 7 data indicate even more water molecules with zero displacement within a pore, consistent with the increase in biomass and clogged pores relative to Day 3. The Day 7 data show fewer molecules with displacements greater than the pore scale in the range of 241 μm to ~2000 μm than Day 3 but indicate more large displacements. The tails of the distributions are more visible in the log scale of Fig. 4(b) and show the increasing persistence of the long displacement tails as a function of biofilm growth quantifying the channeling effect.

The transition in dispersion dynamics due to the biofilm growth shows excellent qualitative agreement with the theoretical time FADE [21,23,24] plotted for varying α in Fig. 5. The FADE model returns the Galilei invariant normal ADE for $\alpha = 1$. As α decreases the distribution becomes Galilei variant with an increasing peak about zero displacement, Fig. 5(a), analogous to the MR measured propagators as a function of biofilm growth. The model propagators for $\alpha = 1/2$ and $\alpha = 1/10$ demonstrate the same behavior at intermediate and long displacements relative to one another as the Day 3 and Day 7 MR propagators in Fig. 4 respectively. Fig. 6 shows the displacement time dependent propagators for the biofilm impacted porous media and demonstrate that the dynamics are well established by $\Delta = 20$ ms. This is in stark contrast to the normal dispersion in the homogeneous clean bead pack which undergoes a preasymptotic regime. The MR propagator data thus provide direct measurement of the biofilm growth induced transition from a homogeneous to a heterogeneous porous media. The data visualizes an increase in the complexity of the porous media due to bioactivity in the sense defined by Goldenfeld and Kadanoff [26], a divergence from normal transport statistics. The homogeneous clean porous media has relatively uniform pore size and permeability which generate normal Gaussian dynamics.

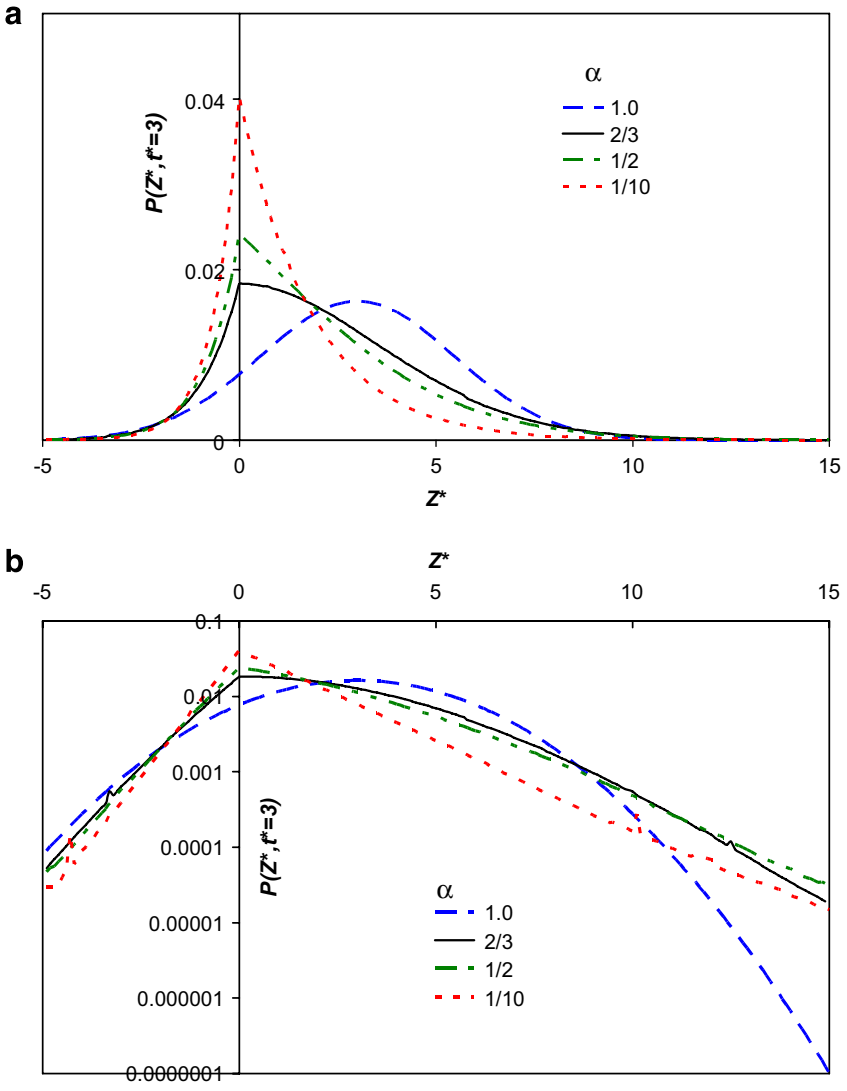

Fig. 5. Theoretical propagators based on the time fractional advection diffusion equation in linear (a) and log (b) scale.

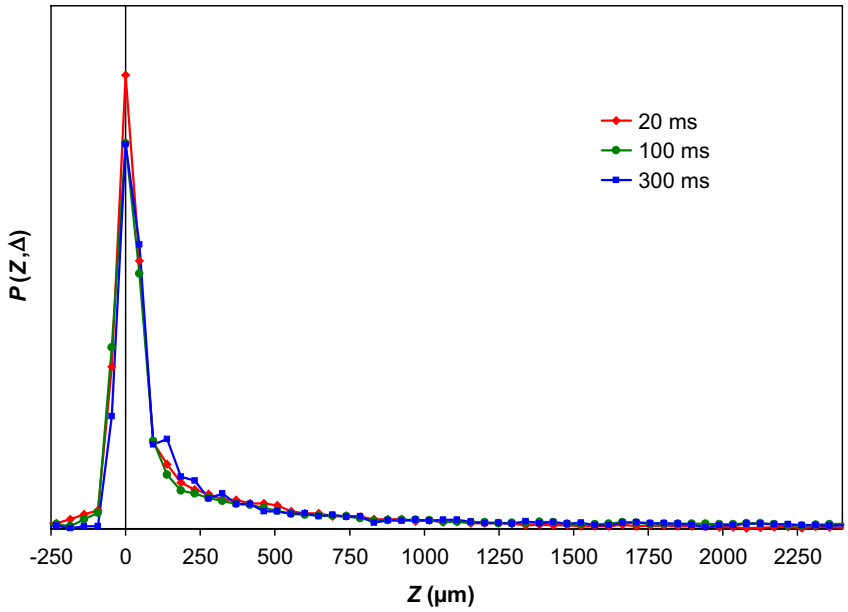

Fig. 6. Propagators of motion for the axial displacement for a biofilm impacted bead pack as a function of displacement observation time Δ taken under flow conditions with an average tube velocity of 1.42 mm/s.

The biofilm growth induces a heterogeneous structural transition with variable pore sizes and permeability variations over a hierarchy of length scales that generate a non-Gaussian displacement distribution.

The biofouling induced structural transition is evidenced by analysis of the $\Delta = 300$ ms data in the q-space Fourier reciprocal space to displacement, Fig. 7 [6]. The Day 1 data show a large decay indicative of the loss of correlation of the dynamics of a Gaussian process followed by a flow induced diffraction like coherence peak with a minimum at a wavelength just larger than the reciprocal of the bead diameter [11,48]. The Day 2 data decrease more rapidly at low q but to a lesser absolute extent than Day 1 indicating more correlated dynamics and have a coherence feature that has not quite decayed away completely. Day 3 exhibits a more rapid low q decay than Day 2, again to a lesser

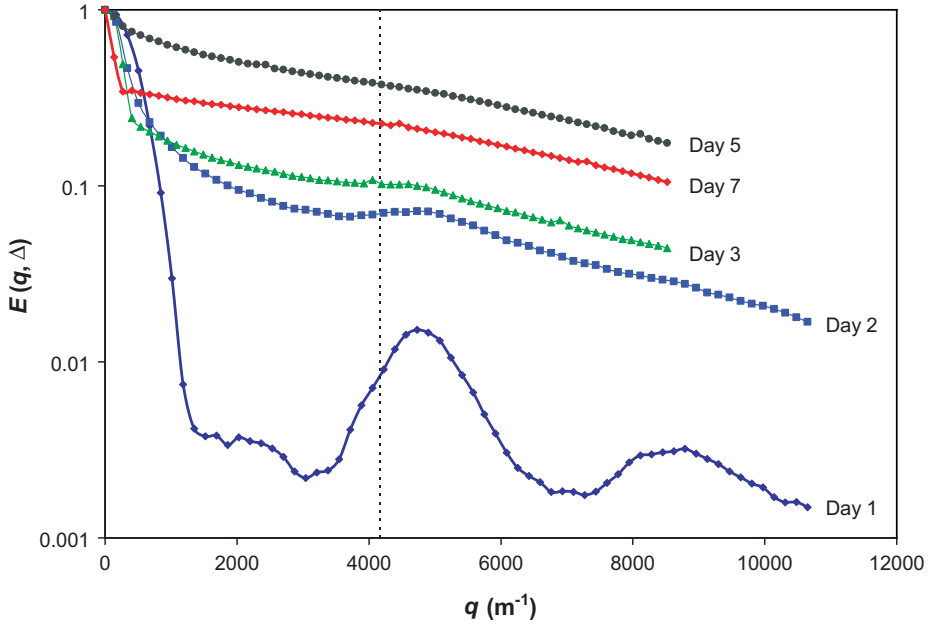

Fig. 7. Reciprocal wavelength to displacement, q-space, plots taken under flow conditions with an average tube velocity of 1.42 mm/s and a displacement observation time $\Delta = 300$ ms. The transition from a clean bead pack (Day 1) to a biofilm impacted bead pack is evident by the decay of the coherence feature which is due to the ordered pore structure. The dashed vertical line is the wavelength corresponding to the reciprocal of the bead diameter.

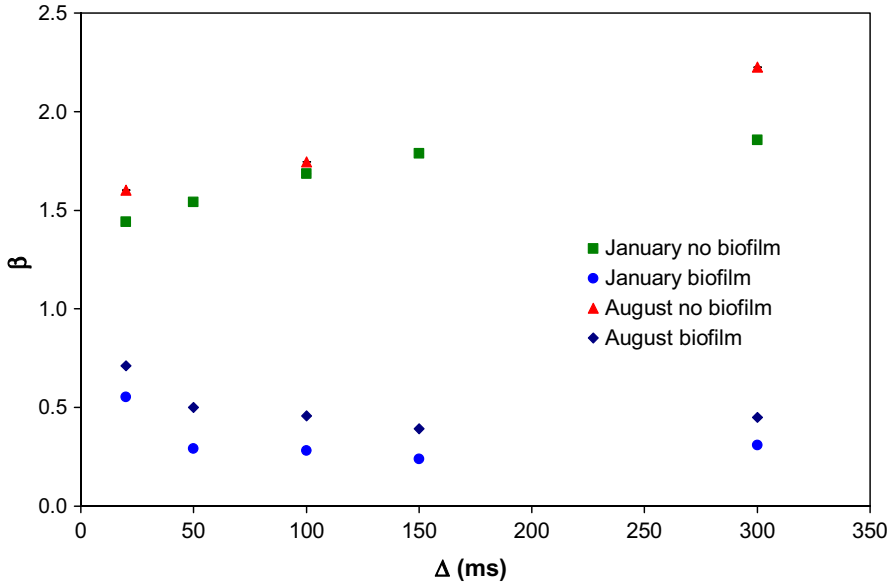

Fig. 8. Stretched exponential, $E(q,\beta)\sim\exp(-cq^{\beta})$, q scaling parameter β as a function of displacement time Δ in the clean and biofilm impacted porous media under flow at an average tube velocity of 1.42 mm/s.

value, and shows just the slightest hint of the initial Day 1 homogeneous structure induced coherence feature. Finally by day 5 any indication of the diffraction effect due to structural order is gone. Note that the Day 5 data decays less than the Day 7 data. This indicates more biomass on Day 5 than Day 7 and the occurrence of a sloughing event between Day 5 and Day 7.

The power law nature of the tails of the propagators in Fig. 4 are quantified by the parameter β in stretched exponential fits of the low q data as a function of observation time, $E(q,\Delta)\sim\exp(-cq^{\beta})$ [6,39]. For the clean porous media propagators in Fig. 3, the pre-asymptotic transition from a Cauchy-like to a Gaussian distribution involves a transition in q-space scaling, Fig. 8, from exponential at short times $\beta\sim 1$ to Gaussian $\beta\sim 2$ in the asymptotic limit. Note the difference in the asymptotic β for the two runs due to packing differences. The biofilm impacted dispersion data exhibits decreasing β with increasing observation time. The stretched exponential in low q-space corresponds to the power law behavior of the propagator tails since the Fourier relationship provides the scaling $P(Z,\Delta)\sim Z^{-(1+\beta)}$. The transition in β at $\Delta=300$ ms from $\sim$2 to $\sim$0.4 due to biofilm growth quantifies the transition in the dispersion dynamics to a scale invariant distribution [39].

6. Conclusions

The impact of biofilm growth on the hydrodynamic dispersion dynamics in porous media can be modeled using a time FADE. MR data provide non-invasive measurement of the pore scale dynamics and biofilm accumulation using velocity imaging and magnetic relaxation weighted imaging respectively. The displacement length and time scale dependent dispersion dynamics are directly measured by PGSE MR. The propagators measured as a function of biofilm growth quantify the transition from normal to anomalous transport. The transition in dynamics for the model bead pack studied indicates a change in the porous media from homogeneous to heterogeneous. The biofilm growth thus increases the complexity [26] of the system. The analysis of the PGSE MR data in both the propagator and q-space provides complementary information on the dynamics and provides a powerful experimental technique for the study of CTRW and FADE models of anomalous transport.

Acknowledgements

This research was supported in part by the Office of Science (BER) US Department of Energy (DE-FG02-03ER63576), a National Science Foundation ADVANCE Award to S.L.C. (DMI-0340709) and a National Science Foundation CAREER Award to J.D.S (CTS-0348076). Acknowledgement is made to the Donors of the American Chemical Society Petroleum Research Fund for partial support of this research. J.P.G acknowledges Ph.D. Fellowship support from the Inland Northwest Research Alliance.

References

[1] Cunningham AB, Characklis WG, Abedeen F, Crawford D. Influence of biofilm accumulation on porous media hydrodynamics. Environ Sci Technol 1991;25:1305–11.
[2] Wanner O, Cunningham AB, Lundman R. Modeling biofilm accumulation and mass transport in a porous medium under high substrate loading. Biotechnol Bioeng 1995;47:703–12.
[3] van As H, Lens P. Use of 1 H NMR to study transport processes in porous biosystems. J Ind Microbiol Biotechnol 2001;26:43–52.
[4] Potter K, Kleinberg RL, Brockman FJ, McFarland EW. Assay for bacteria in porous media by diffusion-weighted NMR. J Magn Reson B 1996;113:9–15.

[5] Hoskins BC, Fevang L, Majors PD, Sharma MM, Georgiou G. Selective imaging of biofilms in porous media by NMR relaxation. J Magn Reson 1999;139:67–73.
[6] Seymour JD, Gage JP, Codd SL, Gerlach R. Anomolous fluid transport in porous media induced by biofilm growth. Phys Rev Lett 2004;93(19):198103.
[7] Brown S, Caprihan A, Hardy R. Experimental observation of fluid flow channels in a single fracture. J Geophys Res – Solid Earth 1998;103(B3):5125–32.
[8] Dijk P, Berkowitz B, Bendel P. Investigation of flow in water-saturated rock fractures using nuclear magnetic resonance imaging (NMRI). Water Resour Res 1999;35(2):347–60.
[9] Dijk P, Berkowitz B, Yechieli Y. Measurement and analysis of dissolution patterns in rock fractures. Water Resour Res 2002;38(2):1013.
[10] Seto K, Hollenshead JT, Watson AT, Chang CTP, Slattery JC. Determination of permeability distributions using NMR velocity imaging. Transp Porous Media 2001;42:351–88.
[11] Seymour JD, Callaghan PT. Flow-diffraction structural characterization and measurement of hydrodynamic dispersion in porous media by PGSE NMR. J Magn Reson A 1996;122:90–3.
[12] Kutsovsky YE, Scriven LE, Davis HT, Hammer BE. NMR imaging of velocity profiles and velocity distributions in bead packs. Phys Fluids 1996;8(4):863–71.
[13] Ding A, Candela D. Probing nonlocal tracer dispersion in flows through random porous media. Phys Rev E 1996;54:656–9.
[14] Lebon L, Oger L, Leblond J, Hulin JP, Martys NS, Schwartz LM. Pulsed gradient NMR measurements and numerical simulation of flow velocity distribution in sphere packings. Phys Fluids 1996;8(2):293–301.
[15] Seymour JD, Callaghan PT. Generalized approach to NMR analysis of flow and dispersion in porous medium. AIChE J 1997;43:2096–111.
[16] Stapf S, Packer KJ, Graham RG, Thovert J-F, Adler PM. Spatial correlations and dispersion for fluid transport through packed glass beads studied by pulsed field-gradient NMR. Phys Rev E 1998;58(5):6206–21.
[17] Manz B, Alexander P, Gladden LF. Correlations between dispersion and structure in porous media probed by nuclear magnetic resonance. Phys Fluids 1999;11(2):259–67.
[18] Tallarek U, Vergeldt FJ, van As H. Stagnant mobile phase mass transfer in chromatographic media: intraparticle diffusion and exchange kinetics. J Phys Chem B 1999;103:7654–64.
[19] Berkowitz B, Scher H. Anomalous transport in random fracture networks. Phys Rev Lett 1997;79(20):4038–41.
[20] Benson DA, Wheatcraft SW, Meerschaert MM. Application of a fractional advection–dispersion equation. Water Resour Res 2000;36(6):1403–12.
[21] Metzler R, Klafter J. The random walk's guide to anomalous diffusion: a fractional dynamics approach. Phys Rep 2000;339:1–77.
[22] Scher H, Shlesinger MF, Bendler JT. Time-scale invariance in transport and relaxation. Phys Today 1991(January):26–34.
[23] Compte A. Continuous time random walks on moving fluids. Phys Rev E 1997;55(6):6821–31.
[24] Metzler R, Compte A. Generalized diffusion–advection schemes and dispersive sedimentation: a fractional approach. J Phys Chem B 2000;104(16):3858–65.
[25] Berkowitz B, Klafter J, Metzler R, Scher H. Physical pictures of transport in heterogeneous media: advection–dispersion, random-walk and fractional derivative formulations. Water Resour Res 2002;38(10):1112–91.
[26] Goldenfeld N, Kadanoff LP. Simple lessons from complexity. Science 1999;284:87–9.
[27] Kimmich R. Strange kinetics, porous media and NMR. Chem Phys 2002;284:253–85.
[28] Taylor GI. Diffusion by continuous movements. Proc Lond Math Soc 1921;20(ser. 2):196–212.
[29] van Kampen NG. Stochastic processes in physics and chemistry. Amsterdam: North-Holland; 1992.
[30] Kubo R, Toda M, Hashitsume N. Statistical physics II: nonequilibrium statistical mechanics. Berlin: Springer-Verlag; 1991.
[31] Taylor GI. Dispersion of soluble matter in solvent flowing slowly through a tube. Proc R Soc London, A 1953;219:186–203.
[32] Mazo RM. Brownian motion: fluctuations, dynamics and applications. New York: Oxford; 2002. p. 289.
[33] Cushman JH, Bennethum LS, Hu BX. A primer on upscaling tools for porous media. Adv Water Resour 2002;25:1043–67.
[34] Brenner H. Macrotransport processes: Brownian tracers as stochastic averagers in effective-medium theories of heterogeneous media. J Stat Phys 1991;62(5/6):1095–119.
[35] Bhattacharya RN, Gupta VK. On the Taylor–Aris theory of solute transport in a capillary. SIAM J Appl Math 1984;44(1):33–9.
[36] Koch DL, Brady JF. A non-local description of advection-diffusion with application to dispersion in porous media. J Fluid Mech 1987;180:387–403.
[37] Cushman JH, Hu BX, Ginn TR. Nonequilibrium statistical mechanics of preasymptotic dispersion. J Stat Phys 1994;75:859–78.
[38] Bouchaud J-P, Georges A. Anomalous diffusion in disordered media: statistical mechanisms, models and applications. Phys Rep 1990;195(4&5):127–293.
[39] Shlesinger MF, Zaslavsky GM, Klafter J. Strange kinetics. Nature 1993;363:31–7.
[40] Kenkre VM, Montroll EW, Shlesinger MF. Generalized master equations for continuous time random walks. J Stat Phys 1973;9(1):45–50.
[41] Sahimi M, Hughes BD, Scriven LE, Davis HT. Stochastic transport in disordered systems. J Chem Phys 1983;78(11):6849–64.
[42] Dentz M, Cortis A, Scher H, Berkowitz B. Time behaviour of solute transport in heterogeneous media: transition from anomalous to normal transport. Adv Water Resour 2004;27:155–73.
[43] Cushman JH, Ginn TR. Fractional advection dispersion equation: a classical mass balance with convolution-Fickian flux. Water Resour Res 2000;36(12):3763–6.
[44] Seymour JD, Codd SL, Gjersing EL, Stewart PS. Magnetic resonance microscopy of biofilm structure and impact on transport in a capillary bioreactor. J Magn Reson 2004;167:322–7.
[45] Gjersing EL, Codd SL, Seymour JD, Stewart PS. Magnetic resonance microscopy analysis of advective transport in a biofilm reactor. Biotechnol Bioeng 2005;89(7):822–34.
[46] van den Broeck C. A stochastic description of longitudinal dispersion in uniaxial flows. Physica 1982;112A:343–52.
[47] Codd SL, Manz B, Seymour JD, Callaghan PT. Taylor dispersion and molecular displacements in Poiseuille flow. Phys Rev E 1999;60(4):R3491–4.
[48] Callaghan PT, Codd SL, Seymour JD. Spatial coherence phenomena arising from translational spin motion in gradient spin echo experiments. Concepts Magn Reson 1999;11:181–202.
[49] Callaghan PT. Principles of nuclear magnetic resonance microscopy. New York: Oxford University Press; 1991.
[50] Edzes HT, van Dusschoten D, van As H. Quantitative T_2 imaging of plant tissues by means of multi-echo MRI microscopy. Magn Reson Imaging 1998;16(2):185–96.
[51] Li T-Q, Seymour JD, Powell RL, McCarthy KL, Odberg L, McCarthy MJ. Turbulent flow studied by time averaged NMR imaging: measurements of velocity profile and turbulent intensity. Magn Reson Imaging 1994;12(6):923–34.
[52] Stejskal EO, Tanner JE. Spin diffusion measurements: spin echoes in the presence of a time-dependent field gradient. J Chem Phys 1965;42:288.
[53] Boon JP, Yip S. Molecular hydrodynamics. New York: Dover Publications; 1991.
[54] Callaghan PT, Coy A, MacGowan D, Packer KJ, Zelaya FO. Diffraction-like effects in NMR diffusion studies of fluids in porous solids. Nature 1991;351:467–9.

[55] Maier RS, Kroll DM, Bernard RS, Howington SE, Peters JF, Davis HT. Pore-scale simulation of dispersion. Phys Fluids 2000;12:2065–79.
[56] Kandhai D, Hlushkou D, Hoekstra AG, Sloot PMA, van As H, Tallarek U. Influence of stagnant zones on transient and asymptotic dispersion in macroscopically homogeneous porous media. Phys Rev Lett 2002;88(23).
[57] Stapf S, Han S-I, Heine C, Blümich B. Spatiotemporal correlations in transport processes determined by multiple pulsed field gradient experiments. Concepts Magn Reson 2002;14(3):172–211.
[58] Callaghan PT, Manz B. Velocity exchange spectroscopy. J Magn Reson Ser A 1994;106:260–5.
[59] Callaghan PT, Codd SL. Flow coherence in a bead pack observed using frequency domain modulated gradient NMR. Phys Fluids 2001;13:412–27.
[60] Callaghan PT, Stepisnik J. Generalized analysis of motion using magnetic field gradients. Adv Mag Opt Res 1996;19:325–88.
[61] Caprihan A, Seymour JD. Correlation time and diffusion coefficient imaging: application to a granular flow system. J Magn Reson 2000;144:96–107.
[62] Song YQ, Tang XP. A one-shot method for measurement of diffusion. J Magn Reson 2004;170(1):136–48.
[63] Song YQ, Scheven UM. An NMR technique for rapid measurement of flow. J Magn Reson 2005;172(1):31–5.
[64] Hurlimann MD, Venkataramanan L, Flaum C. The diffusion-spin relaxation time distribution function as an experimental probe to characterize fluid mixtures in porous media. J Chem Phys 2002;117(22):10223–32.
[65] Callaghan PT, Godefroy S, Ryland BN. Diffusion–relaxation correlation in simple pore structures. J Magn Reson 2003;162(2):320–7.
[66] van der Weerd L, Melnikov SM, Vergeldt FJ, Novikov EG, van As H. Modelling of self-diffusion and relaxation time NMR in multi-compartment systems with cylindrical geometry. J Magn Reson 2002;156(2):213–21.
[67] Walters III MC, Roe F, Bugnicourt A, Franklin MJ, Stewart PS. Contributions of antibiotic penetration, oxygen limitation, and low metabolic activity to tolerance of *pseudomonas aeruginosa* biofilms to ciprofloxacin and Tobramycin. Antimicrob Agents Chemother 2003;47(1):317–23.